Journal of Computer-Aided Molecular Design, 10 (1996) 31–40
ESCOM

J-CAMD 321

Molecular modelling and conformational analysis of a $GABA_B$ antagonist

Bernard Pirard* and François Durant

Laboratoire de Chimie Moléculaire Structurale, Facultés Universitaires Notre-Dame de la Paix, rue de Bruxelles 61, B-5000 Namur, Belgium

Received 4 July 1995
Accepted 21 September 1995

Keywords: Pharmacophoric pattern; Crystallographic database; Molecular dynamics; Similarity

Summary

Crystallographic database studies and molecular dynamics simulations in different media have enabled us to sample the conformational space of a $GABA_B$ antagonist. As a result, we have defined a pharmacophoric pattern for $GABA_B$ antagonists. This study has led us to compare the conformational preferences deduced from database studies and molecular dynamics simulations. The influence of the medium on the conformations has also been investigated.

Introduction

Within the central and peripheral nervous systems, γ-aminobutyric acid (GABA) can bind to at least two different kinds of receptors, $GABA_A$ and $GABA_B$. $GABA_A$ receptors are involved in fast synaptic transmission, while $GABA_B$ receptors act in a modulatory fashion [1,2]. $GABA_B$ agonists have therapeutic potential in certain respiratory diseases such as asthma, while antagonists could be useful in the treatment of cognitive disorders, absence epilepsy and possibly in depression [2–4].

To date, R-(−)-γ-amino-β-(*p*-chlorophenyl)-butyric acid (baclofen) has been considered as a lead compound. The *p*-chlorophenyl moiety has been replaced by a furan, thiophen, benzo[*b*]furan, benzo[*b*]thiophen or quinoline ring [5,6]. These variations led to the discovery of specific $GABA_B$ agonists and antagonists, 3-heteroaromatic baclofen analogues [7–9]. The most potent among these exhibit IC_{50} values in the micromolar range [5,6]. Previously, conformational analysis has enabled us to identify six features that are necessary for $GABA_B$ affinity of 3-heteroaromatic baclofen analogues: (i) a carboxylate group; (ii) a primary ammonium group; (iii) a mean distance between ionized moieties of about 4.6 Å; (iv) an aromatic ring (phenyl, thienyl, benzo[*b*]furan) bound to C^{β}; (v) a lipophilic substituent in the para position (phenyl) or in position 5 (thienyl and benzo[*b*]furan), a position sensitive to steric bulk; and (vi) another lipophilic substituent in position 7 (benzo[*b*]furan) [10].

However, Froestl and co-workers [4,11] have recently described a new class of potent (IC_{50} values in the nanomolar range) phosphinic $GABA_B$ antagonists, which apparently do not show close structural similarity to 3-heteroaromatic baclofen analogues. Five moieties are necessary for $GABA_B$ affinity of phosphinic antagonists: (i) a phosphinate group; (ii) a secondary ammonium group bound to C^{γ}; (iii) a hydroxyl group bound to C^{β}; (iv) a bulky lipophilic group bound to the phosphorus atom; and (v) a second lipophilic group bound to the nitrogen atom [11].

The primary aim of the present work was to assess whether these phosphinic antagonists may match the pharmacophoric pattern of 3-heteroaromatic baclofen analogues. As no crystal structure is available for phosphinic antagonists, the 3D structure of CGP55845 (Fig. 1), the most rigid and potent among this class of compounds, was built from fragments retrieved from the Cambridge Structural Database (CSD). As a result, we have gained insight into the conformational preferences of CGP55845. Then, molecular dynamics (MD) simulations were carried out to further explore the conformational space of this $GABA_B$ antagonist. Another aim of

*To whom correspondence should be addressed.

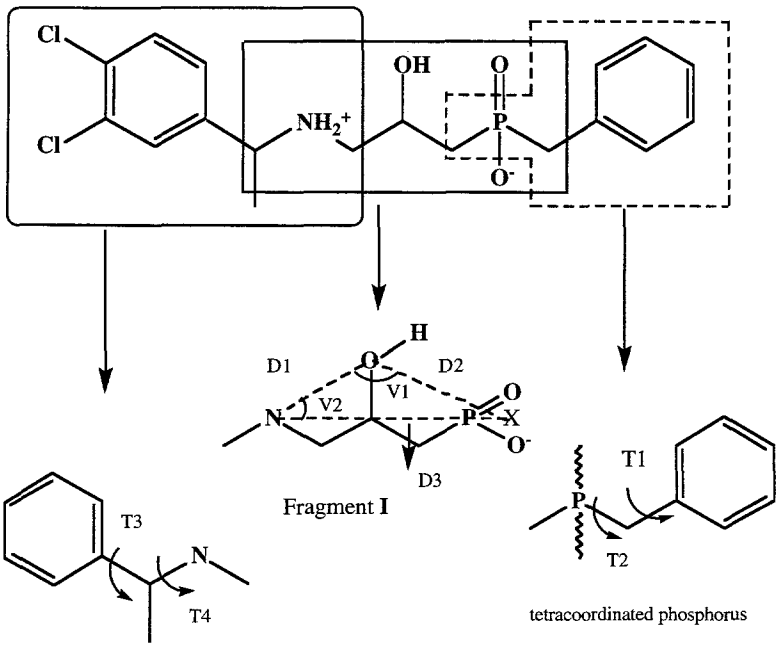

Fig. 1. Planar structural formula of CGP55845. This structure was divided into three fragments, **I–III**, which were searched through the CSD. The definition of the geometrical descriptors relevant for conformational analysis is also given; X is the mean position of the phosphinate group.

this work was to compare the conformational preferences deduced from both approaches. In order to simulate different environmental conditions, different dielectric constants were considered.

Materials and Methods

Taking account of the advantages and limitations of the current methodologies for conformational analysis [12], we considered an approach based on statistical analysis of fragment conformations, followed by MD simulations. These simulations were performed on the whole molecule.

Model building and statistical analysis of fragment conformations

The planar structure of CGP55845 was divided into three fragments (Fig. 1), which were searched through the CSD (v. 5.08, August 1994) [13].

Fragment **I** (Fig. 1) was not located within the CSD; therefore we performed a similarity searching, as implemented in the CSD [14]. This searching mode allows retrieval of those molecules in the CSD that are structurally most similar to an input 2D structure, the query structure [15,16]. Two query structures (Fig. 2a) were considered here. The similarity between both query structures and every entry in the CSD was measured by the Tanimoto coefficient (T): $T = N_c/(N_q + N_t - N_c)$, where N_c is the number of bit screens common to the query and any given entry, N_q is the number of bit screens in the query structure, and N_t is the number of bit screens in any given entry. Then, the conformation of the entry displaying a maximum T value and the same pattern of functional groups as fragment **I** was taken as a template. For the other internal coordinates of fragment **I**, we considered mean interatomic distances and mean valence angles derived from the CSD.

Both fragments **II** and **III** (Fig. 1) were located within the CSD. The hits were submitted to geometrical and statistical analyses. The latter analyses primarily aimed to derive mean geometries and to identify the most frequent conformations. At this point, we should mention that those crystal structures displaying R factors larger than 0.070 were discarded.

The three fragments were then assembled to obtain conformers of CGP55845. The torsion angles around bonds connecting fragments **I–II** and **I–III** were fixed at 180°. For this purpose, we used the ZEDIT program [17] running on an IBM RISC 6000 at the Scientific Computing Facility (SCF) Center of the University of Namur. The different routines of the CSD system were also run on an IBM RISC 6000 machine.

Molecular dynamics simulations

The fragmental approach described above assumes that a given fragment exhibits the same conformation in diverse molecules. In addition, the conformational preferences deduced from the CSD may be biased by both the crystal packing forces and the limited structural diversity of the entries containing the searched fragment [12]. As a

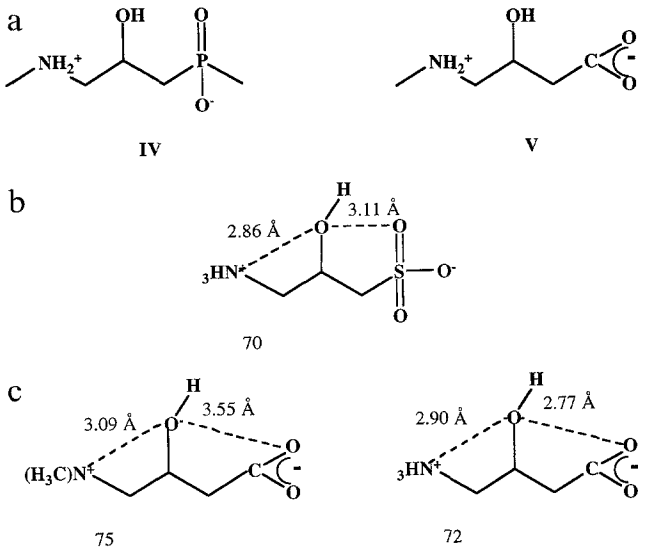

Fig. 2. Planar structural formulae of (a) the query structures; and (b, c) the templates, considering **III** and **IV**, respectively, as query. The values of the Tanimoto coefficient (T, %) are also presented. The REF codes are available as supplementary material from the authors.

consequence, we performed MD simulations [18] in order to overcome the biases of the fragmental approach.

Starting from a 3D model of CGP55845 deduced from the fragmental approach, we performed a sequence of molecular mechanics (MM) minimizations of the initial conformation, high-temperature (500 K) molecular dynamics (HTMD) runs, MM minimizations of selected conformers, room temperature (300 K) molecular dynamics (RTMD) runs of these selected conformers and final MM minimizations. This sequence was repeated under different environmental conditions. For this purpose, dielectric constants (ε) of 80 and 10.3 were used to roughly simulate an aqueous phase and an octanol medium, respectively. Water and octanol are often considered to study partition phenomena [19].

At each stage of the simulation sequence, the energy was evaluated by the CFF91 force field as implemented in the DISCOVER 2.9.5/94.0 program [20]. The CFF91 force field, a second generation force field, has been shown to be more accurate than first generation ones [21–23]. Before each HTMD simulation, two minimization runs were performed using steepest descents and conjugate gradients until the maximum derivatives were respectively less than 1.0 kcal $Å^{-1}$ and 0.1 kcal $Å^{-1}$. The minimized structure was submitted to a 20 ps HTMD (500 K) simulation. As the starting conformation does not have a major influence on the generated conformers [18], we carried out only one HTMD simulation in each environmental medium. The coordinates produced by HTMD were stored and minimized every ps, giving 21 conformers. The minimization strategy has been described above. However, the convergence criterion was fixed at 0.1 kcal $Å^{-1}$ for both the steepest descent and the conjugate gradients minimizations. Among the 21 generated conformers, we only considered further those within 5 kcal of the lowest one. Previously, a study of pentapeptides suggested that a threshold of 5 kcal was sufficient to scan their conformational surface [24]. The selected con-

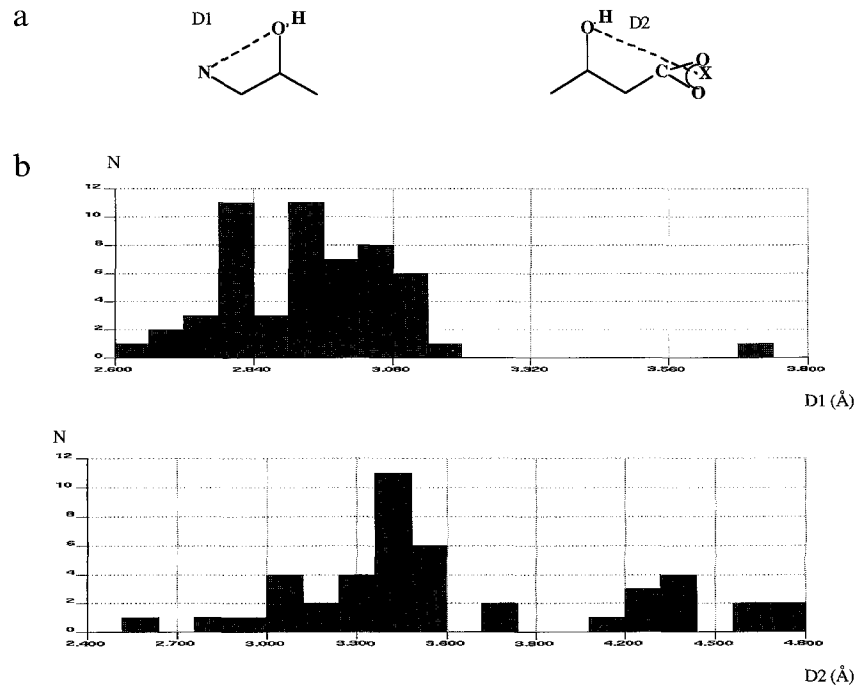

Fig. 3. Statistical analysis of D1 and D2. (a) Fragments searched through the CSD and definitions of D1 and D2 (Å); (b) distributions of D1 and D2. X is the mean position of the carboxylate group. Crystal structures displaying an R factor of more than 0.070 have not been considered. The REF codes and the main characteristics of the distributions are available as supplementary material from the authors.

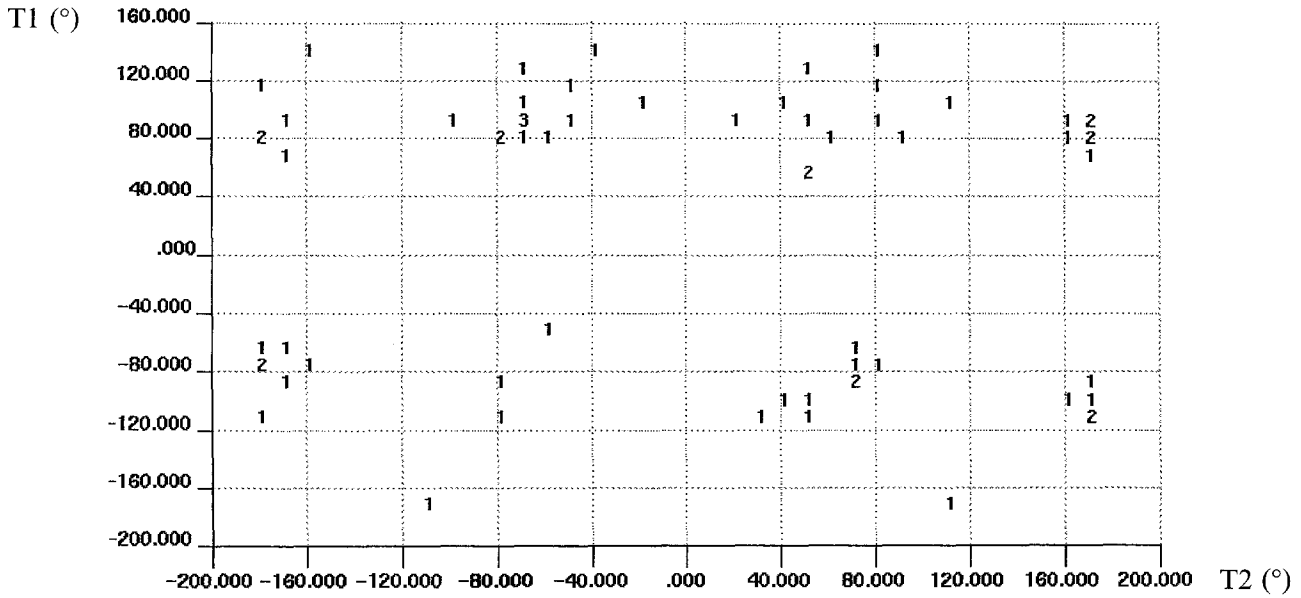

Fig. 4. Variation of T1 versus T2 (°) for fragment **II** (see legend to Fig. 1). The REF codes and the main characteristics of the distribution are available as supplementary material.

formers were submitted to a 20 ps RTMD simulation. The coordinates generated by these runs were processed like those produced by the HTMD simulations. The time step was fixed to 1 fs for each simulation.

The DISCOVER 2.9.5/94.0 program [20] was used for the simulations. Each fs sequence of initial MM minimizations, HTMD (500 K) and RTMD (300 K) simulations and final MM minimizations of selected conformers took 1 h on a Silicon Graphics Indigo II workstation. The results were analyzed by the INSIGHT II [25] program, running on the same workstation.

Results

Model building and statistical analysis of fragment conformations

Three templates of fragment **I** were located within the CSD. As shown in Fig. 2b, their conformations are stabilized by electrostatic interactions between the hydroxyl and both the anionic and cationic moieties. As a consequence, we may reasonably expect the same kind of interactions for fragment **I**. In order to further examine this hypothesis, we have analyzed the distributions of the D1

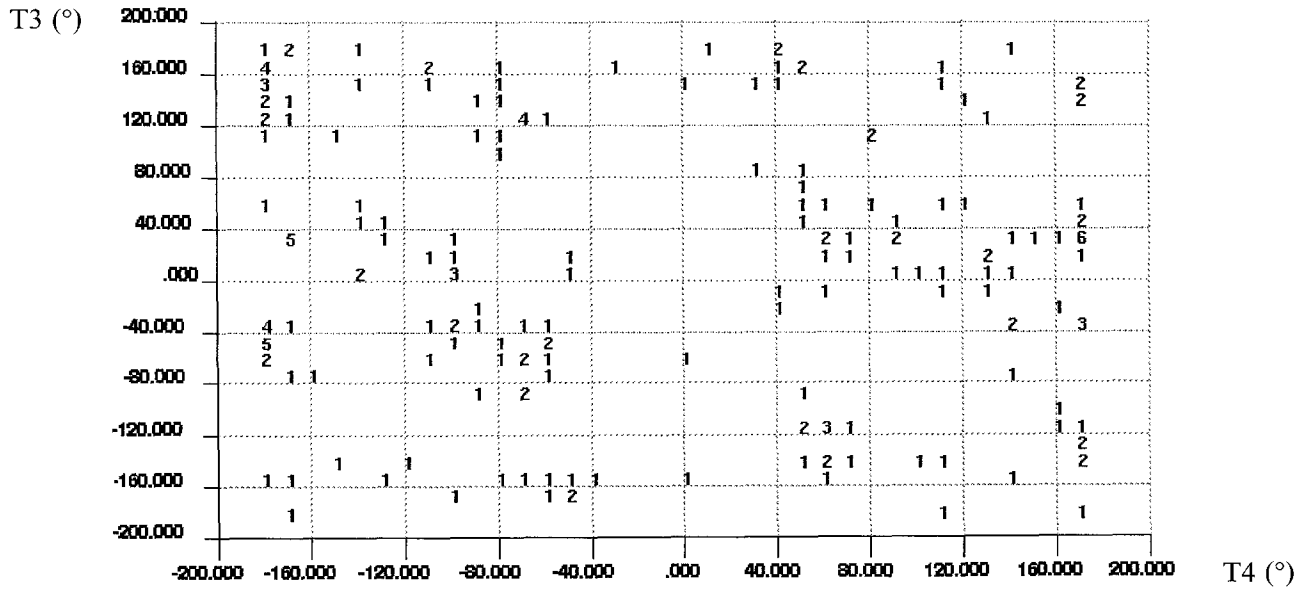

Fig. 5. Variation of T3 versus T4 (°) for fragment **III** (see legend to Fig. 1). The REF codes and the main characteristics of the distribution are available as supplementary material.

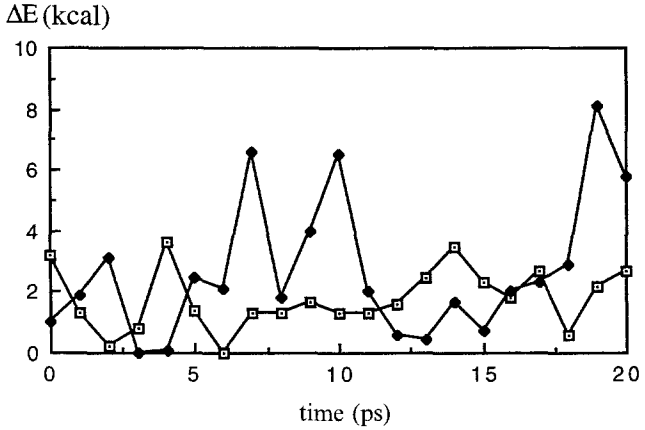

Fig. 6. Fluctuations of the total relative energies (ΔE, kcal) during 20 ps of HTMD simulations (500 K) in an aqueous phase (ε = 80, open squares) and in an octanol environment (ε = 10.3, black squares).

and D2 distances for the fragments shown in Fig. 3a. These fragments were retrieved from the CSD (v. 5.08, August 1994). Within the data sets under study, most of the D1 values (85%; Fig. 3b) are either near the short end of the range or equal to 3.080 Å, while the D2 values show a larger range (Fig. 3b). Consequently, fragment **I** may adopt either *anti* or *gauche* conformations around the C^{α}-C^{β} bond. On the other hand, the conformational preferences around the C^{β}-C^{γ} bond seem to be limited to *gauche* conformations.

For fragment **II**, the distributions of two relevant torsion angles (T1 and T2, Fig. 1) have been considered. The variation of T1 versus T2 is shown in Fig. 4. Most of the T1 values (75%) cluster together between ±80.0° and ± 120.0°, while the T2 values spread mainly in two areas, i.e., $\pm 50.0° \leq T2 \leq \pm 80.0°$ (49%) and $\pm 150.0° \leq T2 \leq \pm 180.0°$ (38%).

For fragment **III**, the distributions of two relevant torsion angles (T3 and T4, Fig. 1) have been analyzed. The variation of T3 versus T4 is shown in Fig. 5. Both of them may adopt a wide range of values. However, frag-

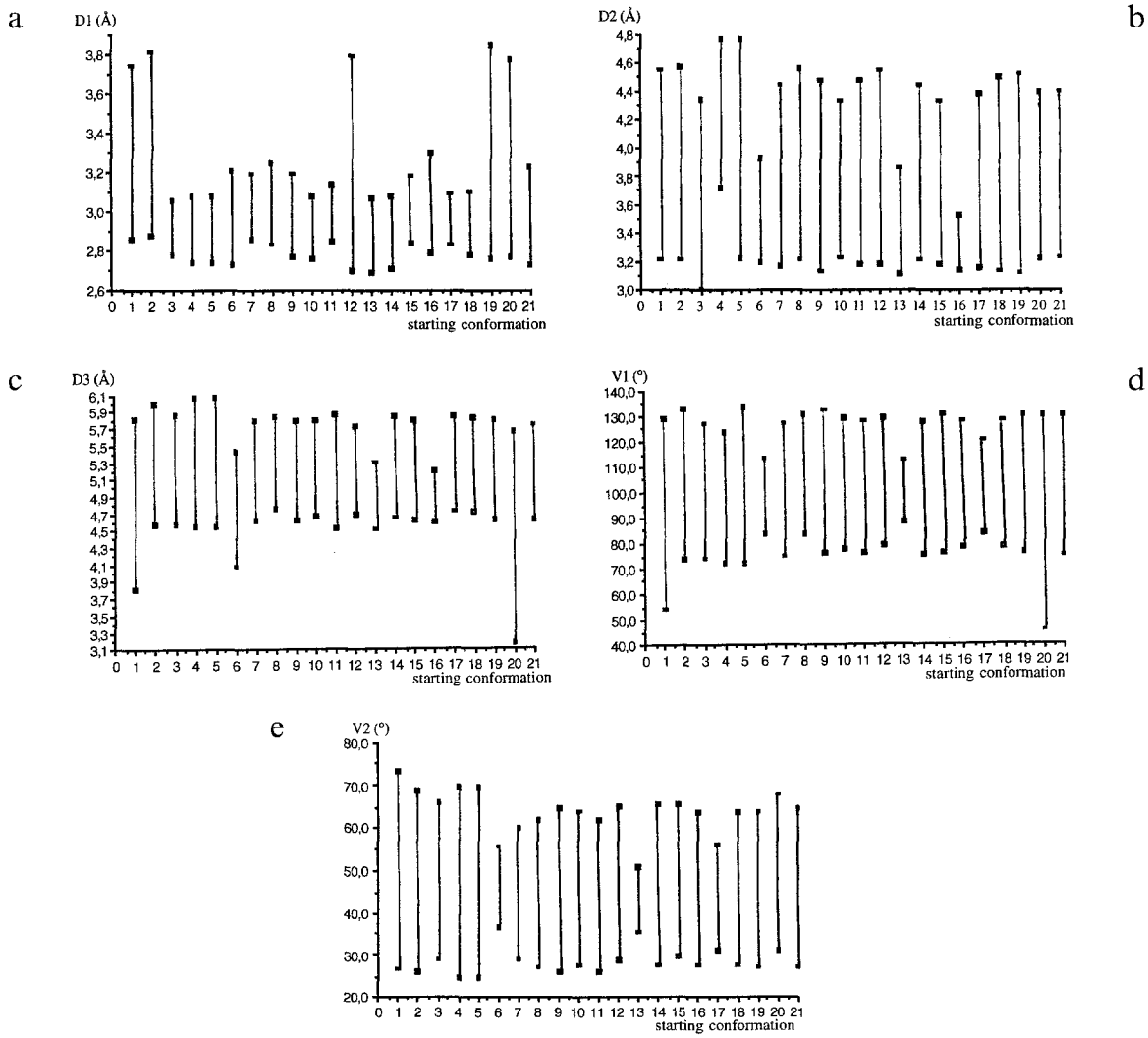

Fig. 7. Range of values explored for the geometrical descriptors of the amino acid chain during RTMD simulations (300 K) in the aqueous phase (ε = 80). (a) Range of D1; (b) D2; (c) D3; (d) V1; and (e) V2.

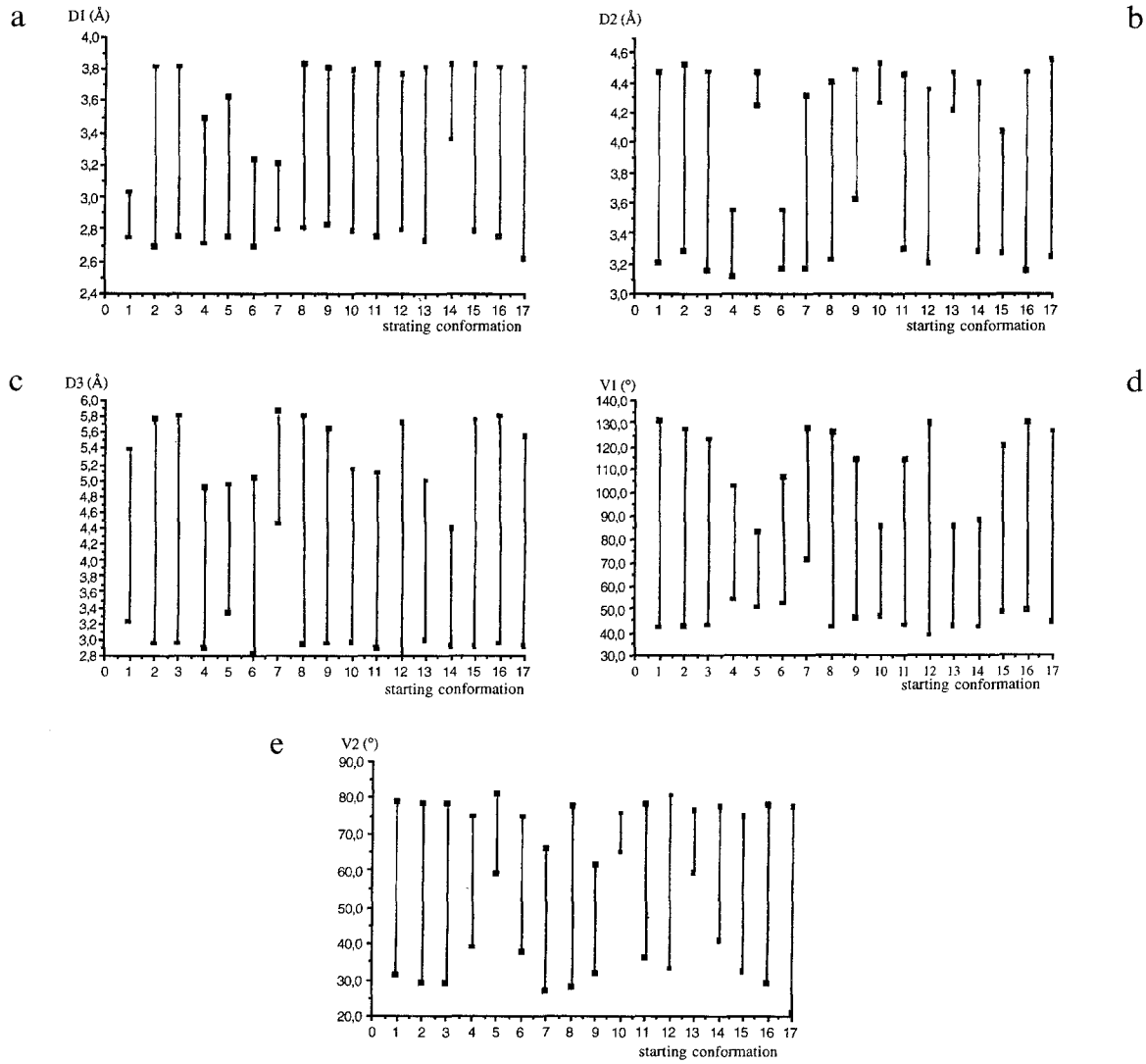

Fig. 8. Range of values explored for the geometrical descriptors of the amino acid chain during RTMD simulations (300 K) in the octanol phase ($\varepsilon = 10.3$). (a) Range of D1; (b) D2; (c) D3; (d) V1; and (e) V2.

ments with T4 values between −40.0° and +40.0° are scarce (7%) within the CSD.

Molecular dynamics simulations

During each HTMD (500 K) simulation, 21 conformers were stored after subsequent minimizations. The variations in their total relative energies as a function of time are shown in Fig. 6. In the aqueous phase ($\varepsilon = 80$), the energies of the whole set of conformers are within a range of 3.6 kcal, while in the octanol environment ($\varepsilon = 10.3$), there are four conformers outside the 5 kcal cutoff. These discrepancies probably arise from the larger contribution of the electrostatic term in an octanol environment. Therefore, 21 and 17 RTMD simulations (300 K) were carried out in the aqueous phase and in the octanol phase, respectively. Within each data set, 21 conformers were stored after subsequent minimizations, giving 441 and 357 conformers, respectively.

Then, nine geometrical descriptors (Fig. 1) were considered in order to quantitatively probe the conformational space of CGP55845. Figures 7–10 show the range of values sampled for each descriptor during the different RTMD simulations. In both media, the compound under study behaves like a flexible molecule. However, the nature of the medium as expressed by ε evidently affects the relative orientations of both the charged and polar groups. In the aqueous phase, the amino acid chain mostly adopts extended conformations, as expressed by minimum values of D3 of over 4.0 Å in most cases and minimum values of V1 of > 70.0° in most cases (19 simulations, see Figs. 7c,d). Moreover, folded conformations ($D3 \leq 4.0$ Å) were found with total relative energies higher than 6 kcal. In other words, extended conformations are preferred in the aqueous phase. This preference arises from the screening of the Coulomb contribution by 1/80. On the other hand, both folded and extended conforma-

tions are likely in the octanol environment (Fig. 8c). They are within 5 kcal of the minimum. The distances between the hydroxylic oxygen and both the cationic (D1) and anionic (D2) groups are also affected by the medium. In the aqueous phase, D2 encompasses a wider range than D1: the variations of D1 are mainly lower than 0.5 Å (16 simulations, Fig. 7a), while D2 shows variations higher than 0.7 Å in 20 simulations (Fig. 7b). In other words, the rotational freedom is more pronounced around the C^{α}-C^{β} bond than around the C^{β}-C^{γ} bond. Previously, similar conclusions were drawn from ^{1}H NMR studies of charged flexible molecules in water [26–28]. However, in the octanol medium, both D1 (12 simulations, Fig. 8a) and D2 (10 simulations, Fig. 8b) mostly show variations of more than 0.7 Å. Whereas the nature of the medium affects the relative orientations of both the charged and the polar moieties, the conformations of the lipophilic groups seem to be less sensitive to the medium (Figs. 9 and 10). In both media, the lipophilic groups exhibit considerable conformational freedom (Figs. 9 and 10).

Discussion

Comparison of conformational preferences deduced from the fragmental approach and MD simulations

Through statistical analyses of fragments retrieved from the CSD, we have gained insight into the conformational preferences of CGP55845. Taking account of the limitations of the fragmental approach [12], we carried out MD simulations in different media. In order to assess the relevance of the fragmental approach, the distributions of several geometrical descriptors (Fig. 1) deduced from the CSD have been compared with those sampled during the RTMD simulations.

The distributions of D1 and D2 (Fig. 3b) derived from the CSD are similar to those explored during the RTMD simulations (Figs. 7a,b and 8a,b). Both the fragmental approach and the RTMD simulations in the aqueous phase predict a larger conformational freedom around the C^{α}-C^{β} bond, as expressed by the wider range of D2 values (Figs. 3b, 7b and 8b). Moreover, within each conformer set generated by the RTMD simulations, the range of D3 values (Figs. 7c and 8c) matches the distribution of D3 deduced from the analysis of γ-amino acids within the CSD (Fig. 11). However, folded conformations (D3 ≤ 4.0 Å) are less frequent in crystals (Fig. 11) than in the octanol environment (Fig. 8c). At this point, we could also note that the isosteric replacement of a carboxylate by a phosphinate does not seem to affect the intercharge distance in γ-amino acids.

Whereas both approaches have yielded similar conformational preferences for the amino acid chain, the RTMD simulations have revealed that the lipophilic groups exhibit a larger conformational freedom than expected on the basis of the fragmental approach. Within the CSD, T1 and T2 cluster together in well-defined areas (Fig. 4), while they can spread over 360.0° during the RTMD simulations (Figs. 9a,b and 10a,b). Both the relatively small number of observations (65, Fig. 4) and their limited structural diversity (no phosphinate group present;

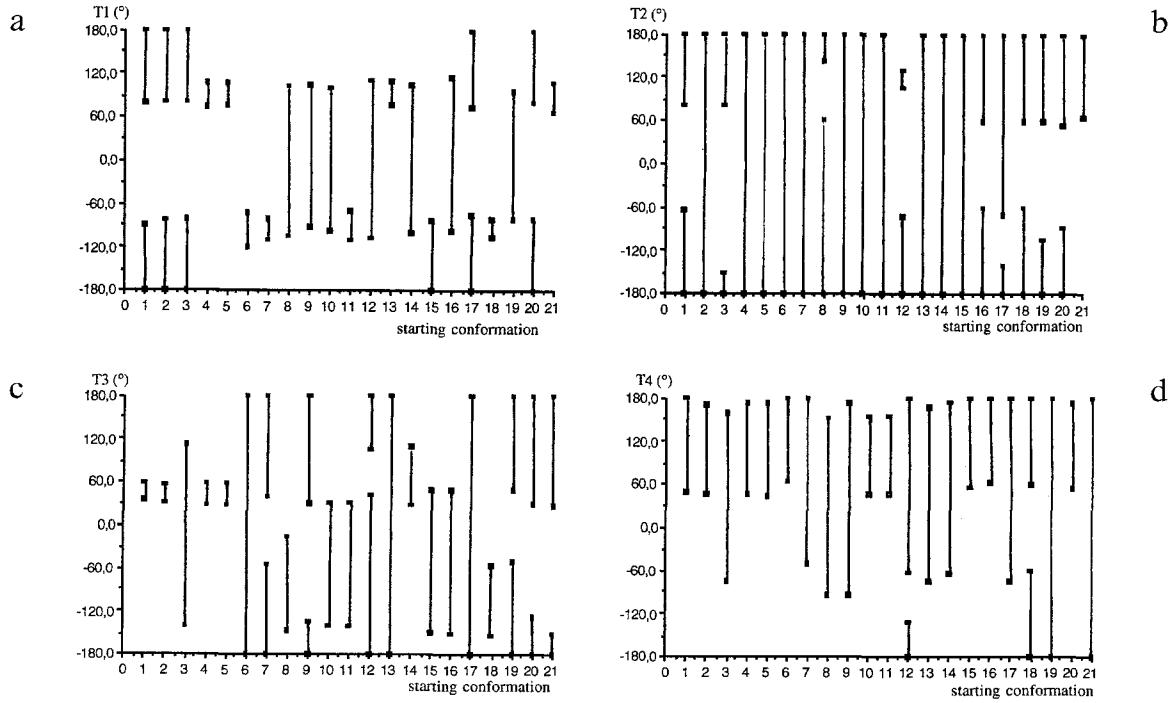

Fig. 9. Range of values explored for the geometrical descriptors of the lipophilic groups during RTMD simulations (300 K) in the aqueous phase (ε = 80). (a) Range of T1; (b) T2; (c) T3; and (d) T4.

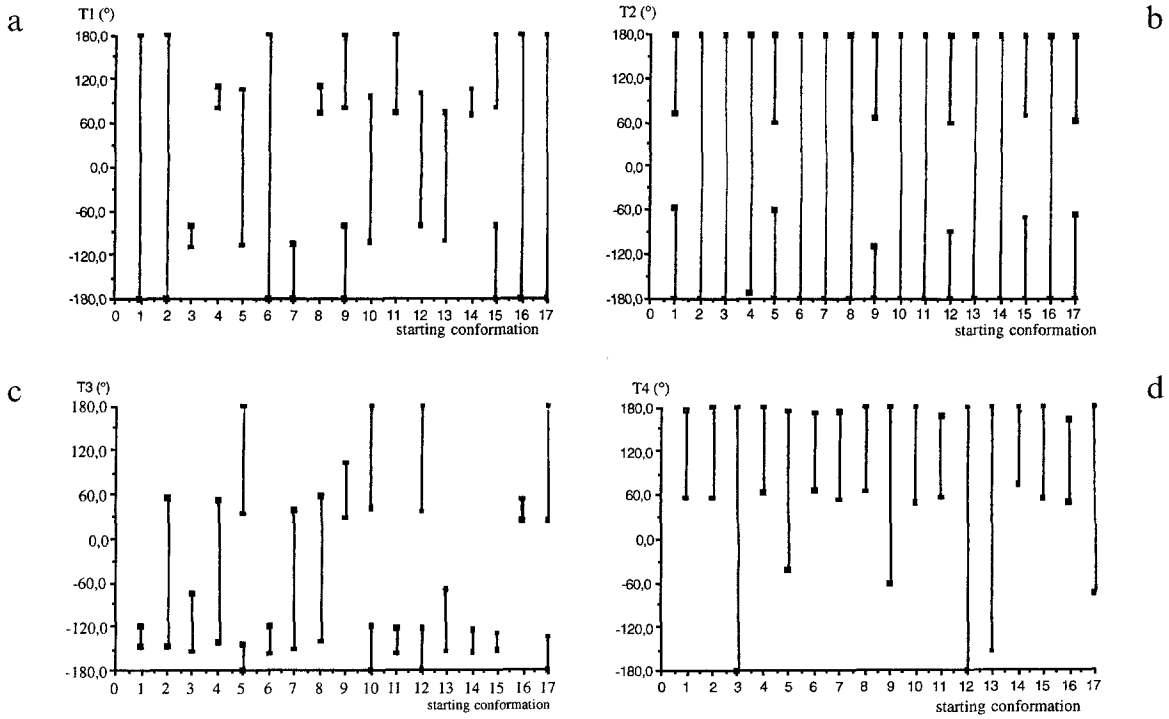

Fig. 10. Range of values explored for the geometrical descriptors of the lipophilic groups during RTMD simulations (300 K) in the octanol phase ($\varepsilon = 80$). (a) Range of T1; (b) T2; (c) T3; and (d) T4.

see the Supplementary Material available from the authors) may account for these discrepancies. As a consequence, the conformational preferences deduced from the statistical analysis of fragment **III** (200 observations, Fig. 5) are in better agreement with the results of the RTMD simulations. Conformations with T3 ≈ 0.0° and T4 ≈ 180.0° were found in neither of the approaches. However, the weakly populated area ($-40.0° \leq T4 \leq 40.0°$) of the diagrams shown in Fig. 5 was sampled during the simulations (Figs. 9d and 10d). As previously stated [29], the use of crystallographic databases has the advantage that they originate from experimental data, but its scope is limited.

$GABA_B$ pharmacophoric pattern (Fig. 12)

CGP55845 is the most potent analog among a class of $GABA_B$ antagonists that apparently do not show close structural similarities with 3-heteroaromatic baclofen analogues. Molecular modelling of CGP55845 has enabled us to gain insight into the conformational preferences for this antagonist. As a result, we have been able

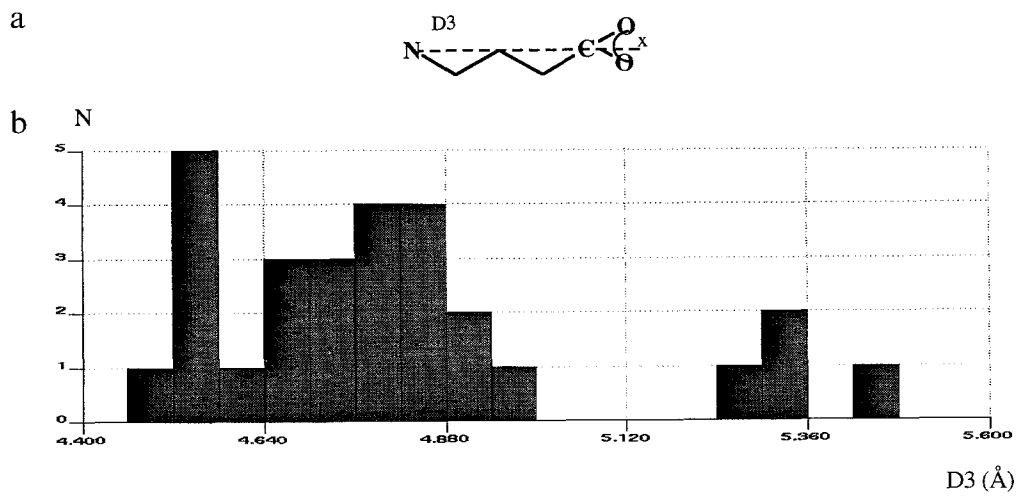

Fig. 11. Statistical analysis of D3. (a) Fragment searched through the CSD and definition of D3 (Å); (b) distributions of D3. In (a) X is the mean position of the carboxylate group. Crystal structures displaying an R factor of more than 0.075 have not been considered. The REF codes and the main characteristics of the distribution are available as supplementary material.

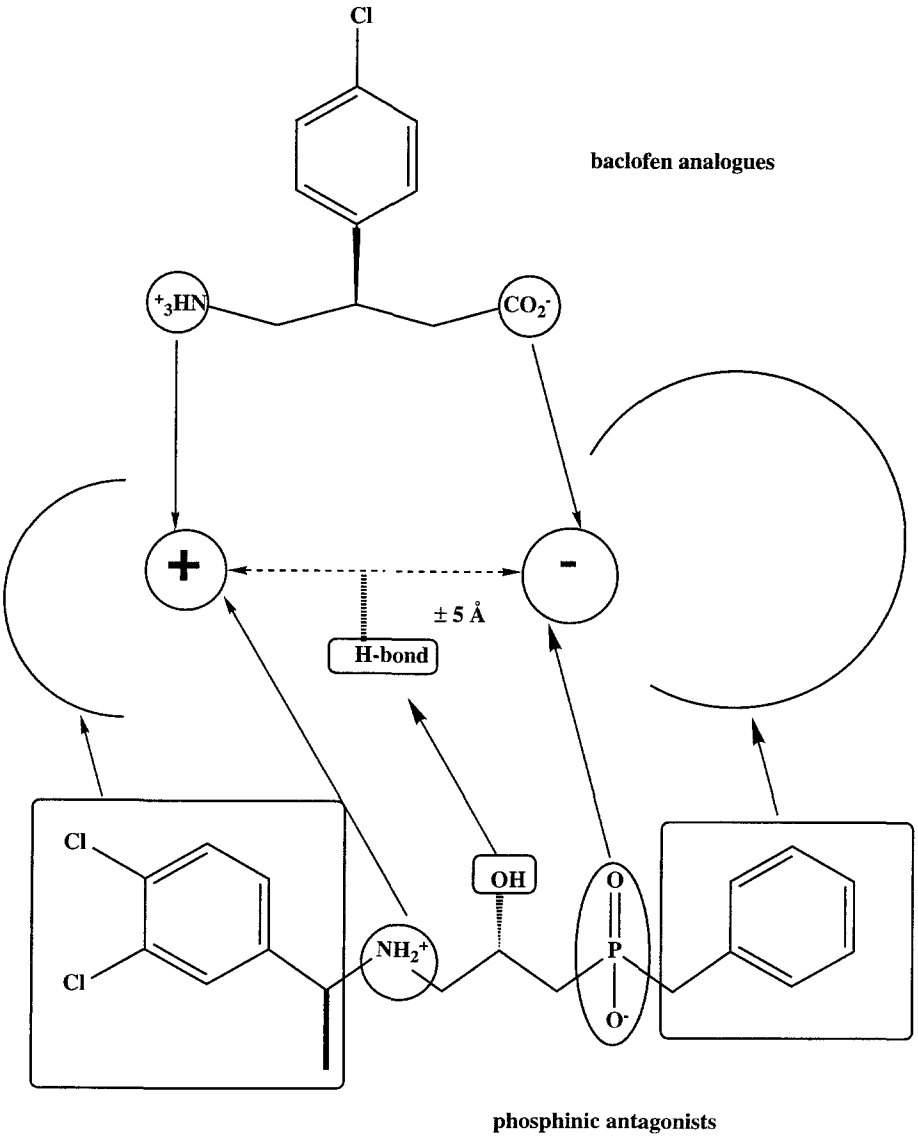

Fig. 12. Pharmacophoric pattern for phosphinic antagonists. The conformational freedom of the lipophilic moieties is sketched by semicircles of different sizes to illustrate different tolerances to steric bulk. The moieties shared by phosphinic antagonists and baclofen analogues are also indicated.

to suggest a pharmacophoric pattern for phosphinic antagonists. The compound under study can exhibit intercharge distances (D3, Figs. 7c and 8c) similar to the mean value (4.6 Å) deduced from conformational analysis of 3-heteroaromatic baclofen analogues [10]. In other words, the charged moieties of both groups of $GABA_B$ ligands may interact with the same residues at the receptor site. This study has also revealed that the hydroxyl group may stabilize the amino acid chain conformation. However, this group is also likely to interact with a specific hydrogen-bond donor or acceptor at the receptor site, as expressed by the stereoselectivity of these antagonists. The *S* configuration is the preferred one for C^{β} [11]. This hypothesis has been previously suggested for other $GABA_B$ ligands [30]. Two lipophilic groups are bound to the phosphorus and nitrogen atoms. Both of these lipophilic groups exhibit considerable conformational freedom. The benzyl group probably interacts with a region of the receptor site that can accommodate a wide range of lipophilic moieties, like alkyl (linear and cyclic), phenyl or alkoxy groups [4,11]. On the other hand, the 3,4-dichlorobenzyl group is likely to interact with a region of the receptor site that is more sensitive to steric bulk, as expressed by the preferred *S* configuration of its α-methyl substituent [11].

Conclusions

The CSD in combination with MD simulations in two media (aqueous and octanol) has been used to sample the

conformational space of CGP55845, a potent $GABA_B$ antagonist. This study has led us to suggest a pharmacophoric pattern for phosphinic antagonists, revealing the following features (Fig. 12): (i) a phosphinate group; (ii) a secondary ammonium group; (iii) a distance between the ionized moieties of about 5 Å; (iv) a hydroxyl group bound to C^{β}, which probably interacts with a specific hydrogen-bond donor or acceptor residue; (v) a lipophilic group bound to the phosphorus atom; and (vi) another lipophilic group (3,4-dichlorobenzyl, possibly substituted by a methyl in the α position) bound to the nitrogen atom. The anionic and cationic groups are shared by both $GABA_B$ agonists and antagonists. The antagonistic nature of these compounds can be explained by the presence of a bulky lipophilic group bound to the phosphorus atom, while the affinity of these antagonists can be enhanced by the presence of two additional groups: the hydroxyl bound to C^{β} and the lipophilic moiety bound to the nitrogen atom.

Acknowledgements

B.P. is indebted to the ADIR society for financial support. The authors also thank the National Belgium Foundation for Scientific Research (FNRS), IBM Belgium and the Facultés Notre-Dame de la Paix (FNDP) for the use of the Namur SCF.

References

1 Krogsgaard-Larsen, P., Frølund, B., Jørgensen, F.S. and Schousboe, A., J. Med. Chem., 37 (1994) 2489.
2 Bowery, N.G., Annu. Rev. Pharmacol. Toxicol., 33 (1993) 109.
3 Chapman, R.W., Hey, J.A., Rizzo, C.A. and Bolser, D.C., Trends Pharmacol. Sci., 14 (1993) 26.
4 Bittiger, H., Froestl, W., Mickel, S.J. and Olpe, H.R., Trends Pharmacol. Sci., 14 (1993) 391.
5 Berthelot, P., Vaccher, C., Musadad, A., Flouquet, N., Debaert, M. and Luyckx, M., J. Med. Chem., 30 (1987) 743.
6 Berthelot, P., Vaccher, C., Flouquet, N., Debaert, M., Luyckx, M. and Brunet, C., J. Med. Chem., 34 (1991) 2557.
7 Hammond, D.L. and Moy, M.L., Eur. J. Pharmacol., 229 (1992) 227.
8 Kerr, D.I.B., Ong, J., Johnston, G.A.R., Berthelot, P., Debaert, M. and Vaccher, C., Eur. J. Pharmacol., 164 (1989) 361.
9 Ong, J., Kerr, D.I.B., Berthelot, P., Vaccher, C., Flouquet, N. and Debaert, M., Eur. J. Pharmacol., 221 (1992) 145.
10 Pirard, B., Paquet, B., Evrard, G., Berthelot, P., Vaccher, C., Ansard, M.H., Debaert, M. and Durant, F., Eur. J. Med. Chem., 30 (1995) 851.
11 Froestl, W., Mickel, S.J., Von Sprecher, G., Bittiger, H. and Olpe, H.R., Pharmacol. Commun., 2 (1992) 52.
12 Leach, A.R., In Lipkowitz, K.B. and Boyd, D.B. (Eds.) Reviews in Computational Chemistry, Vol. 2, VCH, New York, NY, 1991, pp. 1–55.
13 Allen, F.H. and Kennard, O., CDA News, 8 (1993) 31.
14 Allen, F.H., Johnson, O., Macrae, C.F., Smith, M.J., Motherwell, S.W.D., Galloy, J.J., Watson, D.G., Rowland, R.S., Edgington, P.R., Garner, S.E., Davies, J.E. and Mitchell, G.F., CSD System, Vol. 1, Cambridge Crystallographic Data Centre, Cambridge, 1992, pp. 639–645.
15 Willett, P., In Dean, P.M. (Ed.) Molecular Similarity in Drug Design, Blackie Academic & Professional, London, 1995, pp. 110–132.
16 Willett, P., Winterman, V. and Bawden, D., J. Chem. Inf. Comput. Sci., 26 (1986) 36.
17 Vanderveken, D.J. and Vercauteren, D.P., ZEDIT, Facultés Universitaires Notre-Dame de la Paix, Namur, 1992.
18 Auffinger, P. and Wipff, G., J. Comput. Chem., 11 (1990) 19.
19 Rekker, R.F. and Mannhold, R., Calculation of Drug Lipophilicity: The hydrophobic Fragmental Constant Approach, VCH, Weinheim, 1992.
20 DISCOVER, v. 2.9.5/94.0, Biosym Technologies, San Diego, CA, 1994.
21 DISCOVER, v. 2.9.5/94.0, User Guide, Part 1, Biosym Technologies, San Diego, CA, 1994, pp 3.1–3.32.
22 Maple, J.R., Hwang, M.-J., Stockfisch, T.P., Dinur, U., Waldman, M., Ewig, C.S. and Hagler, A.T., J. Comput. Chem., 15 (1994) 162.
23 Maple, J.R., Dinur, U. and Hagler, T., Proc. Natl. Acad. Sci. USA, 85 (1988) 5350.
24 Perez, J.J., Villar, H.O. and Loew, G.H., J. Comput.-Aided Mol. Design, 6 (1992) 175.
25 INSIGHT II, v. 2.3.0, Biosym Technologies, San Diego, CA, 1993.
26 Coluci, W.J., Gandour, R.D. and Mooberry, E.A., J. Am. Chem. Soc., 108 (1986) 7147.
27 Vaccher, C., Berthelot, P., Flouquet, N., Marko, J. and Debaert, M., Spectrochim. Acta, 47 (1991) 1071.
28 Vaccher, C., Berthelot, P., Debaert, M., Vermeersch, G., Guyon, R., Pirard, B., Vercauteren, D.P., Dory, M., Evrard, G. and Durant, F., J. Mol. Struct., 301 (1993) 199.
29 Böhm, H.J., Klebe, G., Lorenz, T., Mietzner, T. and Siggel, L., J. Comput. Chem., 11 (1990) 1021.
30 Falch, E., Hedegaard, A., Nielsen, L., Jensen, B.R., Hjeds, H. and Krogsgaard-Larsen, P., J. Neurochem., 47 (1986) 898.